



Supplement of

Climate and ecology in the Rocky Mountain interior after the early Eocene Climatic Optimum

Rebekah A. Stein et al.

Correspondence to: Rebekah A. Stein (restein@berkeley.edu) and Nathan D. Sheldon (nsheldon@umich.edu)

The copyright of individual parts of the supplement might differ from the article licence.

Supplemental Tables:

Table S1: Paleosol features. Paleosols are stored in ESS labs at the University of Michigan, Ann Arbor, U.S.A.

Sample ID	Paleosol #	Depth (cm)	Horizon	Root traces, rhizoliths	Redox Haloes	Burrows	Peds	Color (descriptive + Munsell)	Texture
19BRWY1UA	1	0	A	Yes				5Y 6/1	
19BRWY1LA	1	-12	A	Yes			Yes	2.5Y 6/1	silt sandstone
19BRWY1LC	1	-18	C					dark brown, 10YR 5/2	silt sandstone, no bedding, not laminated
19BRWY2UA	2	0 to -5	A	Yes	Yes			green grey, 2.5Y 7/3	
19BRWY2UB	2	-25	B			Yes, up to 1 cm		5Y 7/2	
19BRWY2MB	2	-50	B			Yes, up to 1 cm		olive, 5Y 7/2	mudstone
19BRWY2LB	2	-75	B					2.5YR 7/3	
19BRWY2C	2	-85	C	Yes, very fine				dark grey, GLEY1 7/10Y	clay-silt to silty clay, laminated
19BRWY3UA	3	0	A	Yes				brown green, 5Y 7/2	
19BRWY3UB	3	-35	B					grey-brown, 5Y 8/1	silty mudstone
19BRWY3MB	3	-45	B					10YR 7/1	
19BRWY3C	3	-75	C					dark grey, 5Y 7/1	mudstone
19BRWY4UB1	4	0	B	Yes	Yes			10YR 7/2	sandy
19BRWY4UB2	4	-15	B					GLEY1 7/10Y	sandy mudstone
19BRWY4LB	4	-30	B					2.5Y 6/2	shale, mudstone
19BRWY4C	4	-60	C					5Y 8/1	shale, mudstone
19BRWY5UA	5	0	A	Yes				dark grey, green	silty mudstone
19BRWY5UB	5	-20	B	Yes				5Y 7/1	siltstone
19BRWY5MB	5	-35	B					5Y 7/2	
19BRWY5C	5	-80	C					dark grey, 5Y 6/1	massive fine sand mudstone
19BRWY6UA	6	0	A					10YR 7/1	
19BRWY6UB	6	-42	B					5Y 7/1	
19BRWY6MB	6	-72	B					5Y 7/2	shale, mudstone
19BRWY6C	6	-112	C					2.5Y 5/1	shale, mudstone

Table 2. Complete ⁴⁰ Ar/ ³⁹ Ar results														
MAP 215-50														
Laser - Single crystal fusion														
Sample:	BR-6		J-value:	0.0105317	± 0.0000058	(2σ)								
Material:	sanidine and orthoclase													
	File	⁴⁰ Ar/ ³⁹ Ar	±1σ	³⁹ Ar/ ³⁹ Ar	±1σ	³⁶ Ar/ ³⁹ Ar	±1σ	⁴⁰ Ar*/ ³⁹ Ar _K	± 2σ	% ⁴⁰ Ar*	Age (Ma) ± 2σ (Ma)	K/Ca	⁴⁰ Ar* (x e-15 mol)	Included in wtd. Mean
	MAA3467	103.2380 ± 0.2319		0.00155 ± 0.00025		0.00026054 ± 0.0000649		103.15989 ± 0.46509		99.92	1346.26 ± 4.30	277.9	32.62	
	MAA3468	6.2767 ± 0.0127		0.00150 ± 0.00033		0.00043156 ± 0.0000597		6.14745 ± 0.04359		97.94	114.83 ± 0.79	286.8	1.52	
	MAA3470	122.0564 ± 1.9798		2.98467 ± 0.06722		0.00304601 ± 0.0022998		121.63489 ± 4.18671		99.45	1509.47 ± 35.38	0.1	0.72	
	MAA3471	92.9050 ± 0.2016		0.00261 ± 0.00044		0.00051381 ± 0.0000797		92.75144 ± 0.40525		99.83	1247.47 ± 3.95	164.4	21.16	
	MAA3473	2.6685 ± 0.0087		0.01655 ± 0.00077		0.00024881 ± 0.0000818		2.59504 ± 0.05174		97.25	49.36 ± 0.97	26.0	0.43	x
	MAA3474	4.2453 ± 0.0097		0.00143 ± 0.00046		0.00017891 ± 0.0000810		4.19148 ± 0.05206		98.73	79.07 ± 0.96	300.9	0.78	
	MAA3476	56.8838 ± 0.1520		0.00408 ± 0.00048		0.00027627 ± 0.0000910		56.80121 ± 0.30843		99.85	858.29 ± 3.72	105.3	9.56	
	MAA3477	2.2931 ± 0.0063		0.01234 ± 0.00073		0.00006373 ± 0.0000703		2.27457 ± 0.04380		99.19	43.33 ± 0.82	34.9	0.46	
	MAA3479	31.7415 ± 0.0891		0.00453 ± 0.00062		0.00050642 ± 0.0001266		31.59023 ± 0.19278		99.52	525.73 ± 2.79	95.0	3.52	
	MAA3480	2.5574 ± 0.0095		0.01244 ± 0.00104		0.00000765 ± 0.0001293		2.55560 ± 0.07953		99.93	48.62 ± 1.49	34.6	0.29	x
	MAA3482	2.5268 ± 0.0065		0.00458 ± 0.00046		0.00007726 ± 0.0000657		2.50352 ± 0.04131		99.08	47.64 ± 0.78	93.9	0.52	x
	MAA3483	2.5697 ± 0.0092		0.01166 ± 0.00071		0.00007149 ± 0.0001016		2.54879 ± 0.06338		99.18	48.49 ± 1.19	36.9	0.34	x
	MAA3485	2.5571 ± 0.0078		0.01141 ± 0.00086		0.00001604 ± 0.0001028		2.55268 ± 0.06332		99.83	48.56 ± 1.19	37.7	0.35	x
	MAA3486	2.6850 ± 0.0073		0.01448 ± 0.00067		0.00020773 ± 0.0000750		2.62366 ± 0.04707		97.71	49.89 ± 0.88	29.7	0.48	
	MAA3488	93.1071 ± 0.2544		0.00297 ± 0.00063		0.00021251 ± 0.0001121		93.04351 ± 0.51280		99.93	1250.32 ± 4.99	144.9	12.06	
	MAA3489	2.6328 ± 0.0091		0.01504 ± 0.00079		0.00019441 ± 0.0001136		2.57541 ± 0.07018		97.82	48.99 ± 1.32	28.6	0.31	x
	MAA3491	2.6102 ± 0.0084		0.01021 ± 0.00072		0.00020218 ± 0.0000921		2.55008 ± 0.05739		97.70	48.51 ± 1.08	42.1	0.39	x
	MAA3492	11.2200 ± 0.0382		0.00303 ± 0.00087		0.00027801 ± 0.0001359		11.13669 ± 0.11103		99.26	203.01 ± 1.92	142.0	1.14	
Weighted mean age (6 of 18):										48.48 ± 0.60	MSWD:	1.40		
Laser - Single crystal fusion														
Sample:	BR-5		J-value:	0.0105317	± 0.0000058	(2σ)								
Material:	sanidine and orthoclase													
	File	⁴⁰ Ar/ ³⁹ Ar	±1σ	³⁹ Ar/ ³⁹ Ar	±1σ	³⁶ Ar/ ³⁹ Ar	±1σ	⁴⁰ Ar*/ ³⁹ Ar _K	± 2σ	% ⁴⁰ Ar*	Age (Ma) ± 2σ (Ma)	K/Ca	⁴⁰ Ar* (x e-15 mol)	Included in wtd. Mean
	MAA3376	96.1168 ± 0.2027		0.00307 ± 0.00037		0.00055795 ± 0.0000631		95.95010 ± 0.40645		99.83	1278.40 ± 3.90	139.9	30.70	
	MAA3377	4.6954 ± 0.0071		0.00062 ± 0.00015		0.00017428 ± 0.0000333		4.64287 ± 0.02431		98.88	87.39 ± 0.45	693.9	2.52	
	MAA3379	64.0019 ± 0.1045		0.00919 ± 0.00050		0.00013895 ± 0.0000563		63.96099 ± 0.21162		99.94	942.68 ± 2.44	46.8	21.79	
	MAA3380	12.5249 ± 0.0250		0.01160 ± 0.00070		0.00005171 ± 0.0000966		12.50999 ± 0.07627		99.88	226.55 ± 1.30	37.1	2.61	
	MAA3382	4.6101 ± 0.0088		0.00962 ± 0.00037		0.00004221 ± 0.0000484		4.59779 ± 0.03382		99.73	86.56 ± 0.62	44.7	1.64	
	MAA3383	22.8047 ± 0.0417		0.00568 ± 0.00034		0.00015340 ± 0.0000525		22.75891 ± 0.08895		99.80	393.30 ± 1.38	75.7	7.92	
	MAA3385	85.0975 ± 0.1457		0.00019 ± 0.00019		0.00016558 ± 0.0000464		85.04751 ± 0.29253		99.94	1170.76 ± 2.97	2277.4	40.82	
	MAA3386	9.6783 ± 0.0181		0.00652 ± 0.00028		0.00012046 ± 0.0000538		9.64234 ± 0.04831		99.63	177.04 ± 0.85	65.9	3.09	
	MAA3388	12.8873 ± 0.0218		0.00433 ± 0.00023		0.00011876 ± 0.0000452		12.85166 ± 0.05114		99.72	232.36 ± 0.87	99.2	5.15	
	MAA3389	7.8382 ± 0.0169		0.00209 ± 0.00039		0.00026206 ± 0.0000839		7.75960 ± 0.06031		99.00	143.79 ± 1.07	205.3	1.58	
	MAA3391	96.8326 ± 0.2066		0.00253 ± 0.00037		0.00000256 ± 0.0000861		96.83169 ± 0.41643		100.00	1286.84 ± 3.97	170.0	22.08	
	MAA3392	65.9480 ± 0.1289		0.00147 ± 0.00037		0.00038218 ± 0.0000925		65.83351 ± 0.26317		99.83	964.13 ± 3.00	292.7	13.97	
	MAA3394	2.6494 ± 0.0060		0.00895 ± 0.00043		0.00011514 ± 0.0000675		2.61519 ± 0.04200		98.71	49.73 ± 0.79	48.1	0.67	
	MAA3395	3.2970 ± 0.0080		0.00306 ± 0.00035		0.00011273 ± 0.0000856		3.26309 ± 0.05350		98.97	61.85 ± 1.00	140.6	0.64	
	MAA3397	95.8149 ± 0.1603		0.00331 ± 0.00027		0.00051954 ± 0.0000614		95.65970 ± 0.32215		99.84	1275.62 ± 3.09	130.0	32.82	
	MAA3398	76.9668 ± 0.1872		0.00116 ± 0.00044		0.00041005 ± 0.0000947		76.84398 ± 0.37803		99.84	1085.37 ± 4.03	371.0	14.21	
	MAA3400	10.8729 ± 0.0218		0.00294 ± 0.00040		0.00034609 ± 0.0000915		10.76926 ± 0.06970		99.05	196.66 ± 1.21	146.0	2.19	
	MAA3401	76.9950 ± 0.1944		0.00411 ± 0.00065		0.00051714 ± 0.0001189		76.84060 ± 0.39454		99.80	1085.34 ± 4.20	104.5	11.67	
	MAA3403	94.1338 ± 0.2122		0.00178 ± 0.00040		0.00011695 ± 0.0001005		94.09857 ± 0.42848		99.96	1260.56 ± 4.15	241.1	18.60	
	MAA3404	53.1049 ± 0.0917		0.00055 ± 0.00026		0.00014928 ± 0.0000608		53.05983 ± 0.18691		99.92	812.60 ± 2.31	787.3	14.65	
No weighted mean age														
Laser - Single crystal fusion														
Sample:	BR-4		J-value:	0.0105290	± 0.0000053	(2σ)								
Material:	sanidine and orthoclase													
	File	⁴⁰ Ar/ ³⁹ Ar	±1σ	³⁹ Ar/ ³⁹ Ar	±1σ	³⁶ Ar/ ³⁹ Ar	±1σ	⁴⁰ Ar*/ ³⁹ Ar _K	± 2σ	% ⁴⁰ Ar*	Age (Ma) ± 2σ (Ma)	K/Ca	⁴⁰ Ar* (x e-15 mol)	Included in wtd. Mean
	MAA3574	7.0535 ± 0.0145		0.00687 ± 0.00048		0.00002067 ± 0.0000511		7.04732 ± 0.04213		99.91	131.02 ± 0.76	62.6	1.60	
	MAA3575	2.6218 ± 0.0057		0.00771 ± 0.00041		0.00003759 ± 0.0000364		2.61069 ± 0.02459		99.57	49.64 ± 0.46	55.8	0.85	x
	MAA3577	2.6160 ± 0.0066		0.00465 ± 0.00040		0.00005689 ± 0.0000409		2.59881 ± 0.02775		99.34	49.41 ± 0.52	92.4	0.72	x
	MAA3578	73.7417 ± 0.1787		0.00135 ± 0.00031		0.00015680 ± 0.0000549		73.69450 ± 0.35858		99.94	1051.30 ± 3.89	319.1	22.08	
	MAA3580	2.6222 ± 0.0062		0.00594 ± 0.00043		0.00008493 ± 0.0000434		2.59674 ± 0.02864		99.03	49.38 ± 0.54	72.5	0.72	x
	MAA3581	2.7331 ± 0.0060		0.00529 ± 0.00037		0.00010627 ± 0.0000412		2.70123 ± 0.02730		98.83	51.33 ± 0.51	81.3	0.81	
	MAA3583	2.8732 ± 0.0103		0.01801 ± 0.00103		0.00002127 ± 0.0000949		2.86781 ± 0.06026		99.81	54.45 ± 1.13	23.9	0.34	
	MAA3584	114.9851 ± 0.2413		0.00155 ± 0.00038		0.00005588 ± 0.0000753		114.96812 ± 0.48466		99.99	1451.98 ± 4.23	278.1	26.78	
	MAA3586	12.2170 ± 0.1135		0.00207 ± 0.00348		0.00004602 ± 0.0006271		12.20289 ± 0.43781		99.88	221.26 ± 7.48	207.4	0.22	
	MAA3587	63.6550 ± 0.1724		0.00188 ± 0.00038		0.00016469 ± 0.0000772		63.60557 ± 0.34769		99.92	938.40 ± 4.01	228.3	13.11	
	MAA3589	2.6225 ± 0.0075		0.00814 ± 0.00066		0.00011397 ± 0.0000637		2.58860 ± 0.04082		98.71	49.22 ± 0.77	52.8	0.52	x
	MAA3590	2.6022 ± 0.0066		0.00575 ± 0.00051		0.00000498 ± 0.0000571		2.60061 ± 0.03661		99.94	49.45 ± 0.69	74.8	0.57	x
	MAA3592	107.6185 ± 0.2201		0.00464 ± 0.00049		0.00019573 ± 0.0000694		107.56020 ± 0.44187		99.95	1386.23 ± 3.99	92.6	25.07	
	MAA3593	10.1839 ± 0.0259		0.02358 ± 0.00074		0.00020003 ± 0.0000833		10.12572 ± 0.07156		99.43	185.44 ± 1.25	18.2	1.50	
	MAA3595	2.6110 ± 0.0069		0.00673 ± 0.00053		0.00007648 ± 0.0000663		2.58819 ± 0.04190		99.13	49.22 ± 0.79	63.9	0.51	x
	MAA3596	2.6440 ± 0.0096		0.01590 ± 0.00090		0.00009529 ± 0.0001194		2.61634 ± 0.07382		98.95	49.74 ± 1.38	27.0	0.31	x
	MAA3598	3.3061 ± 0.0082		0.00203 ± 0.00036		0.00009427 ± 0.0000582		3.27759 ± 0.03839		99.14	62.10 ± 0.72	211.7	0.77	

[illegible]

Table S3: Descriptions of paleosols. GPS coordinates (locations) and observations for A, B, and C horizons, as well as samples taken and suspected identification included.

	19BRWY1	19BRWY2	19BRWY3	19BRWY4	19BRWY5	19BRWY6
GPS coordinates	41.798926215, -109.58362614, 2028m ASL (3m accuracy)	41.7990789, -109.58532463, 2016m ASL (3m accuracy)	41.79905197, -109.58550286, 2011m ASL (3m accuracy)	41.79994128, -109.58647569, 2008m ASL (3m accuracy)	41.7986239, -109.58589332, 2016m ASL (3m accuracy)	41.7982093, -109.958601308, 2012m ASL (3m accuracy)
A	0 - 15cm, truncated by tan sandstone above. A-horizon characterized by thin dark mudstone with peds, mm-scale rootlets and rhizoliths. Slickensides present	0 - 25cm, Grey green mudstone, kerogenized and oxidized rootlets present. Mostly ~1cm in diameter (few > 2cm). Burrows present, up to 1cm.	0 - 25 cm, Grey-brown-green silty mudstone. Root traces present. Non-calcareous replacement of organic matter by rhizoliths. Some kerogenized rootlets ~2mm	Missing? Or weakly developed.	0 - 20cm, silty mudstone, rare rhizoliths, rare kerogenized roots	0 - 40cm, silty mudstone, Taenidium burrow trace fossil of insect, brownish/reddish rock with some yellow-green brown rootlets.
B	Missing	25 - 70cm, burrows present up to 1cm diameter. Olive colored clay-rich mudstone. Bt or Bw horizon? Clear color change throughout section.	25 - 75cm, grey/brown silty/clay mudstone. Bw/Bg, gleyed, water table? May reclassify color change as Bg. Darker Munsell than A.	0 - 50cm, Drab-haloed rootlets, sandier	20 - 80cm, massive, weakly developed red siltstone with some kerogenized roots (rare) that disappeared entirely around 40 - 45cm.	40 - 105 cm, greenish grey silty mudstone, with drab-haloed roots, dark brown.
C	15 - 18cm, Tan sandstone (similar to that found above A-horizon), Round crevasse Splay? Weak ped development, non-laminated, poorly bedded.	70 - 85cm, Dark-grey, laminated mudstone. Clayey silt to silty clay. Roots penetrate to base, hairlike <1 mm	75 - 90cm, Detrital Plant bits present? Grey shale.	60 cm - 75 cm, Shale	80 - 90 cm, dark grey, massive mudstone. No roots, some mixed in fine sand.	105 cm - unk, grey, dark brown mudstone.
Intervals Sampled	19BRWYUA: 0cm; 19BRWYLA: 12cm; 19BRWY1C: 18cm	19BRWY2UB: 25 cm; 19BRWYMB: 45 cm; 19BRWYLB: 75cm; 19BRWY2C: 85cm	19BRWYUA: 0cm; 19BRWYUB: 35cm; 19BRWYMB: 45cm; 19BRWY3C: 75cm	19BRWY4UB1: 0cm; 19BRWY4UB2: 15cm; 19BRWY4LB: 30cm; 19BRWY4C: 60cm	19BRWY5UA: 0cm; 19BRWY5UB: 20cm; 19BRWY5MB: 35cm; 19BRWY5C: 80cm	19BRWY6UA: 0cm; 19BRWY6UB: 42cm; 19BRWY6MB: 72cm; 19BRWY6C: 112cm
ID	Inceptisol, some horizonation but weak	Histic Inceptisol or green/grey deeply penetrating Alfisol	Parent material and evidence of waterlogging, weak horizonation indicative of Inceptisol	Inceptisol with missing A horizon and sparse roots into B. Likely weakly developed because little color change	Weak development and massive B and C horizons indicate Inceptisol, rootlets and color perhaps poorly developed Alfisol	Weak development, parent material and waterlogging, likely Inceptisol

Supplemental Figures:

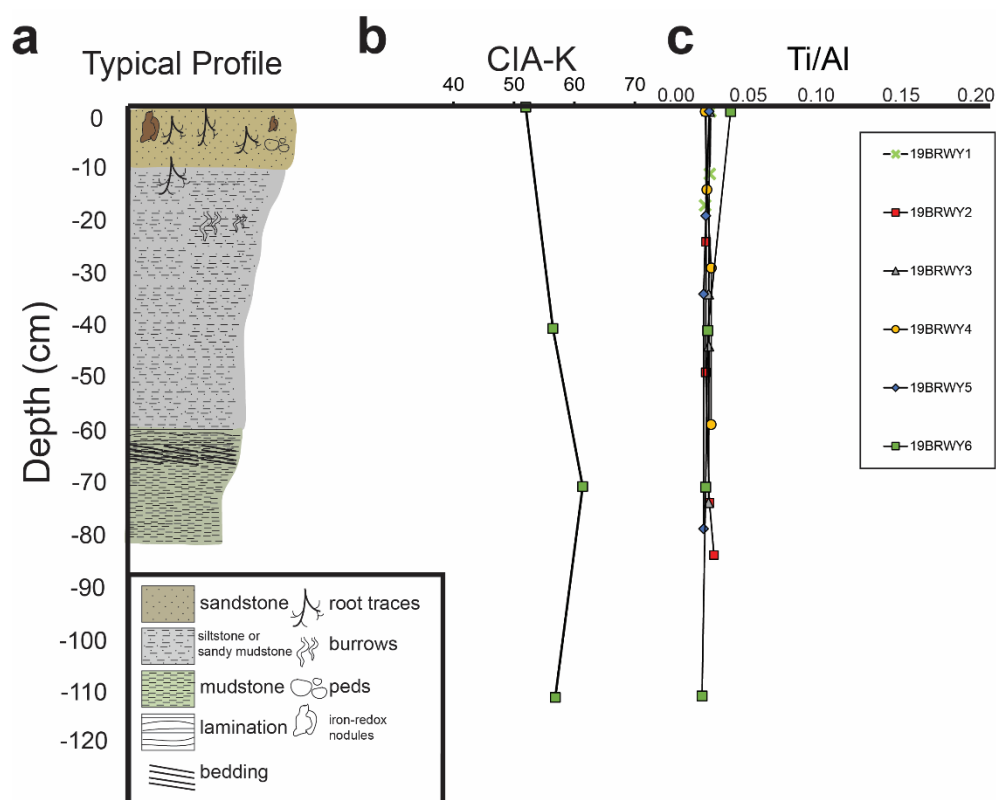


Figure S1 Paleosol features and elements. (a) Average paleosol profile at Blue Rim escarpment based on common horizon depths and features, (b) typical CIA-K over profile, (b) Ti/Al ratio (molar) for all paleosol profiles.

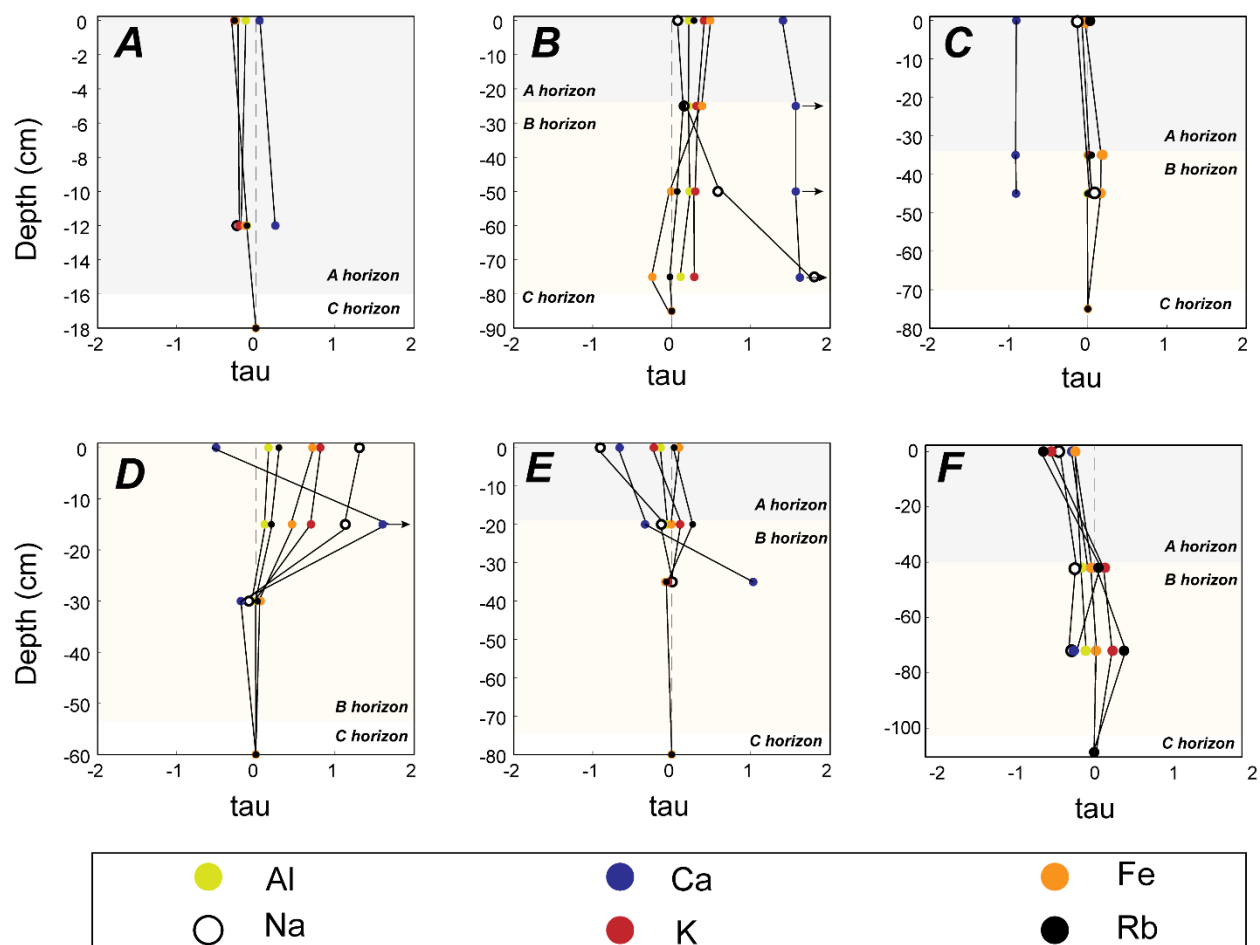


Figure S2 Up profile changes in tau (mobile element transport, see equations 2 and 3, per Chadwick et al. 1990) for Paleosols #1 (A) through #6 (F).

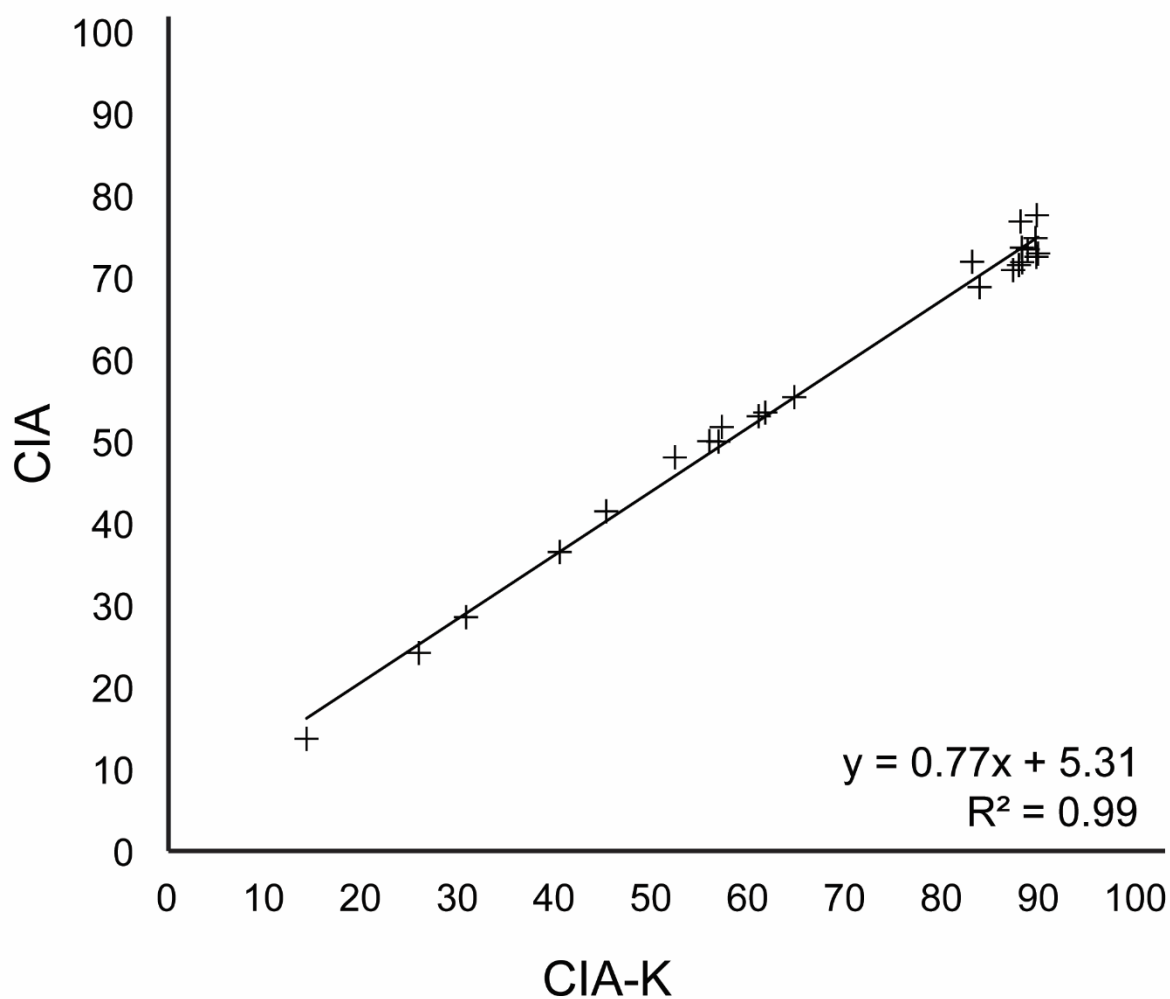


Figure S3 Relationship between CIA-K and CIA for all paleosol bulk geochemistry data, measured by ALS Laboratories in Vancouver, British Columbia, Canada.

More Leaching

(+)

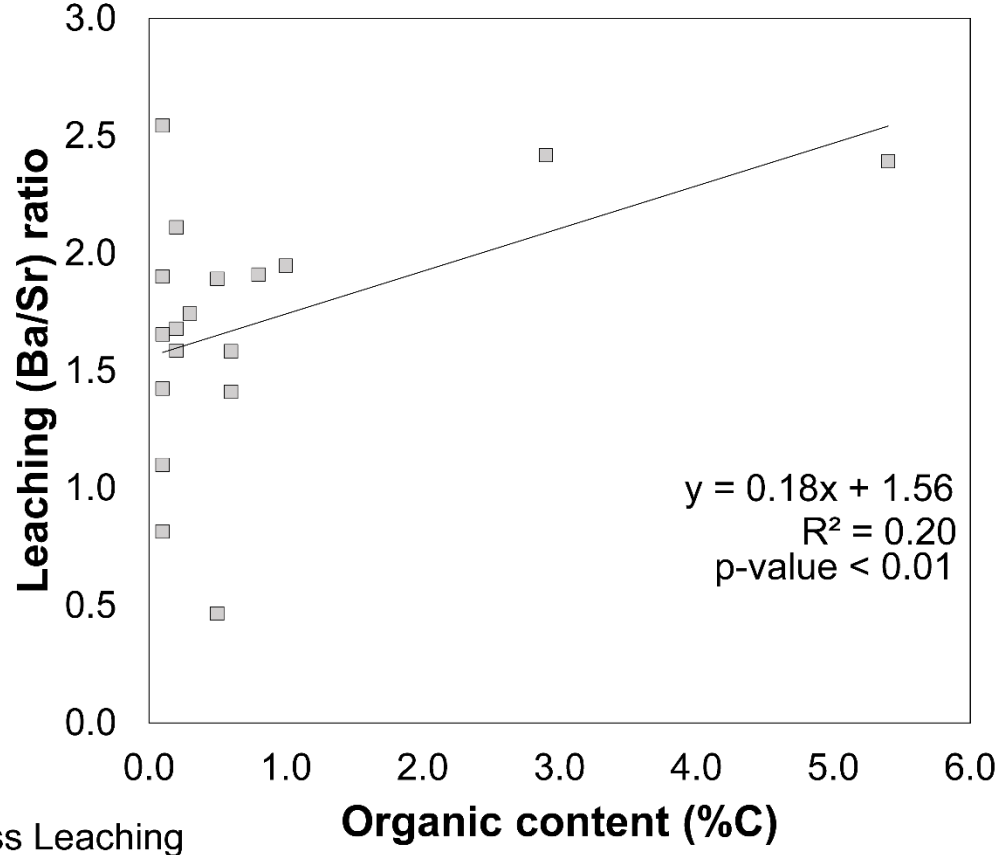


Figure S4 Comparison between organic content in stratigraphic units (%C) and leaching (Ba/Sr ratio).

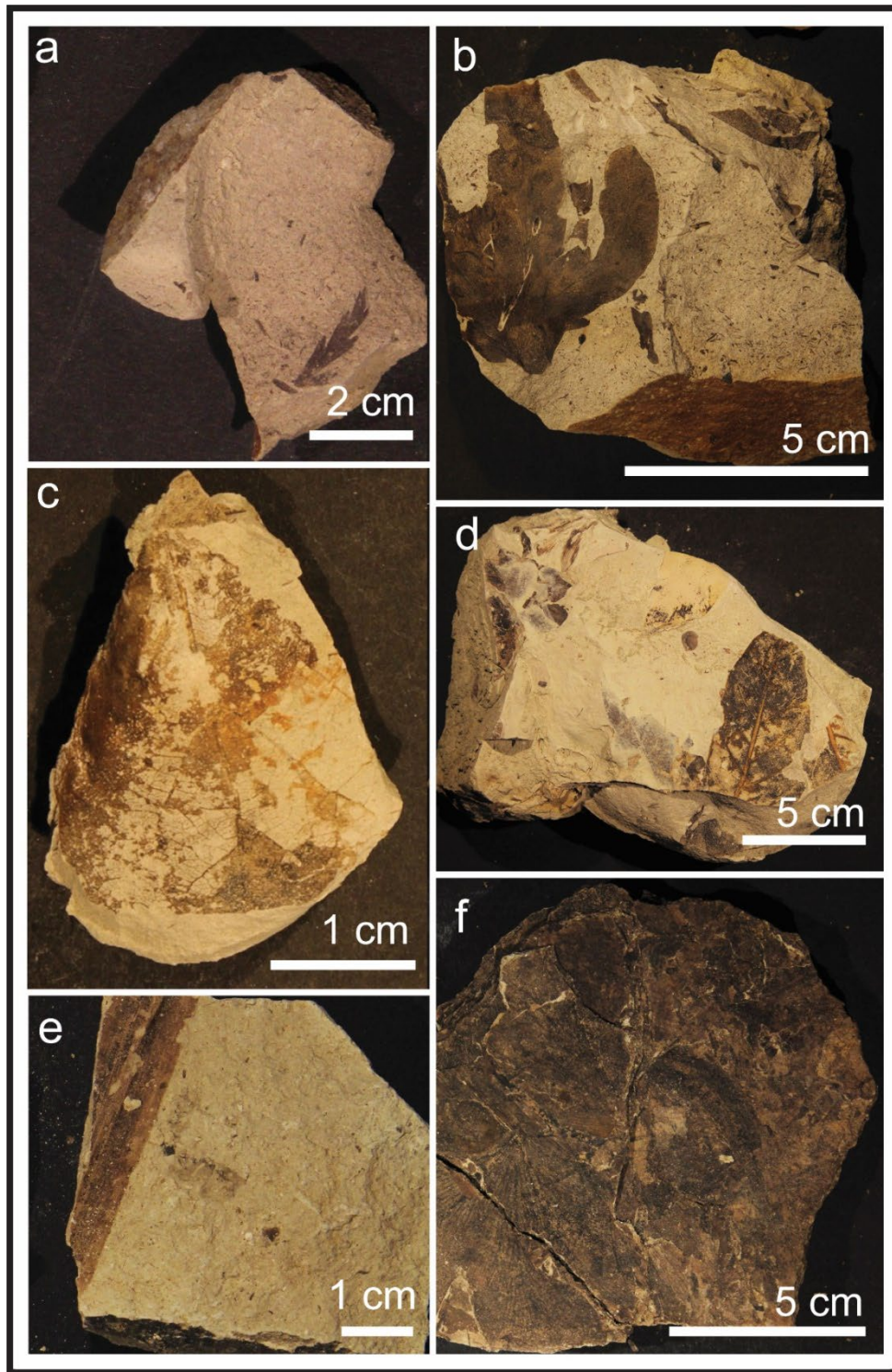


Figure S5 Common plant fossils and preservation types found at the Blue Rim Escarpment (2019): (a) *Lygodium kaulfussi*, (b) *Asplenium* sp. (c) *Populus cinnamomoides*, (d) cf. *Cedrela* sp. (e) unidentified monocot, (f) unidentified organ carbon-rich leaf mat, all sampled at 26 m in the section (see Figs. 3-5).

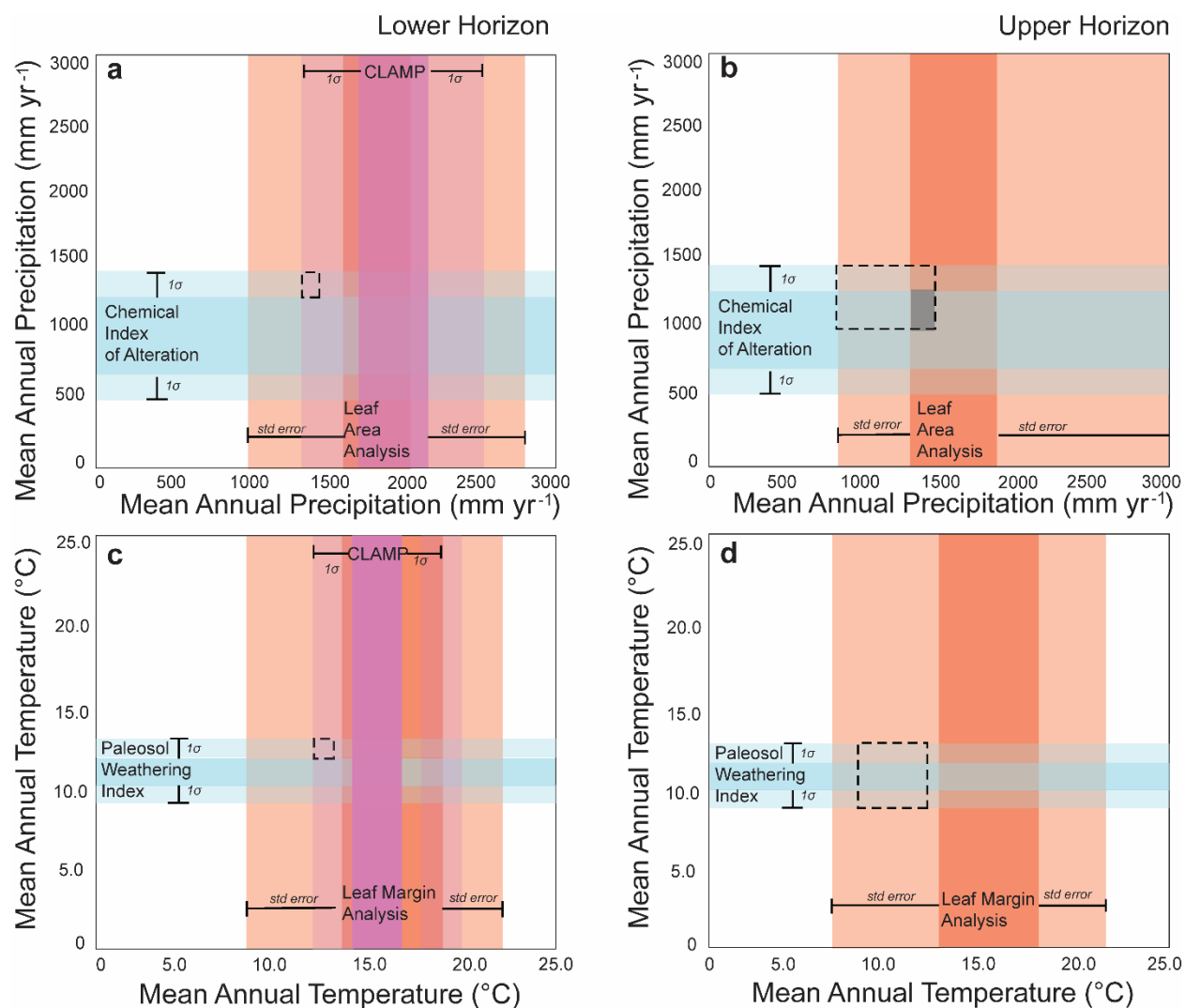


Figure S6 Comparisons of paleoclimate reconstructions using multiple proxies at Blue Rim, southwestern Wyoming. Paleosol-based proxies are shown in blue (y-axis), with opaque blue representing the range of reconstructed precipitation (a-b) and temperature (c-d) and transparent blue shows error for each proxy (1σ for Chemical Index of Alteration and Paleosol Weathering Index). Two plant-based proxies are shown in red (x-axis), with opaque red representing the range of reconstructed precipitation using leaf margin analysis and leaf area analysis based off multiple regional and global equations (e.g., Wolfe 1979; Wing & Greenwood 1993; Wilf 1997; Wilf et al., 1998; Gregory-Wodzicki 2000; Jacobs 2004; Kowalksi & Dilcher 2003; Miller et al., 2006; Peppe et al., 2011), and error (standard error) shown in opaque red. Climate Leaf Analysis Multivariate Program (CLAMP, a & c; e.g., Spicer et al. 2009) is shown in purple, with opaque purple to show the range of reconstructed values based on regional meteorological stations and global reconstructions, and transparent purple showing standard deviation (1σ). CLAMP was not done on the upper horizon. The precipitations and temperatures for which both proxies overlap (within error) are outlined in a dashed box, and grey boxes show the precipitations and temperatures that overlap for reconstructed ranges (excluding error). The Lower (plant macrofossil) Horizon is shown in panels a and c, the Upper (plant macrofossil) Horizon is shown in panels b and d (Allen, 2017b).

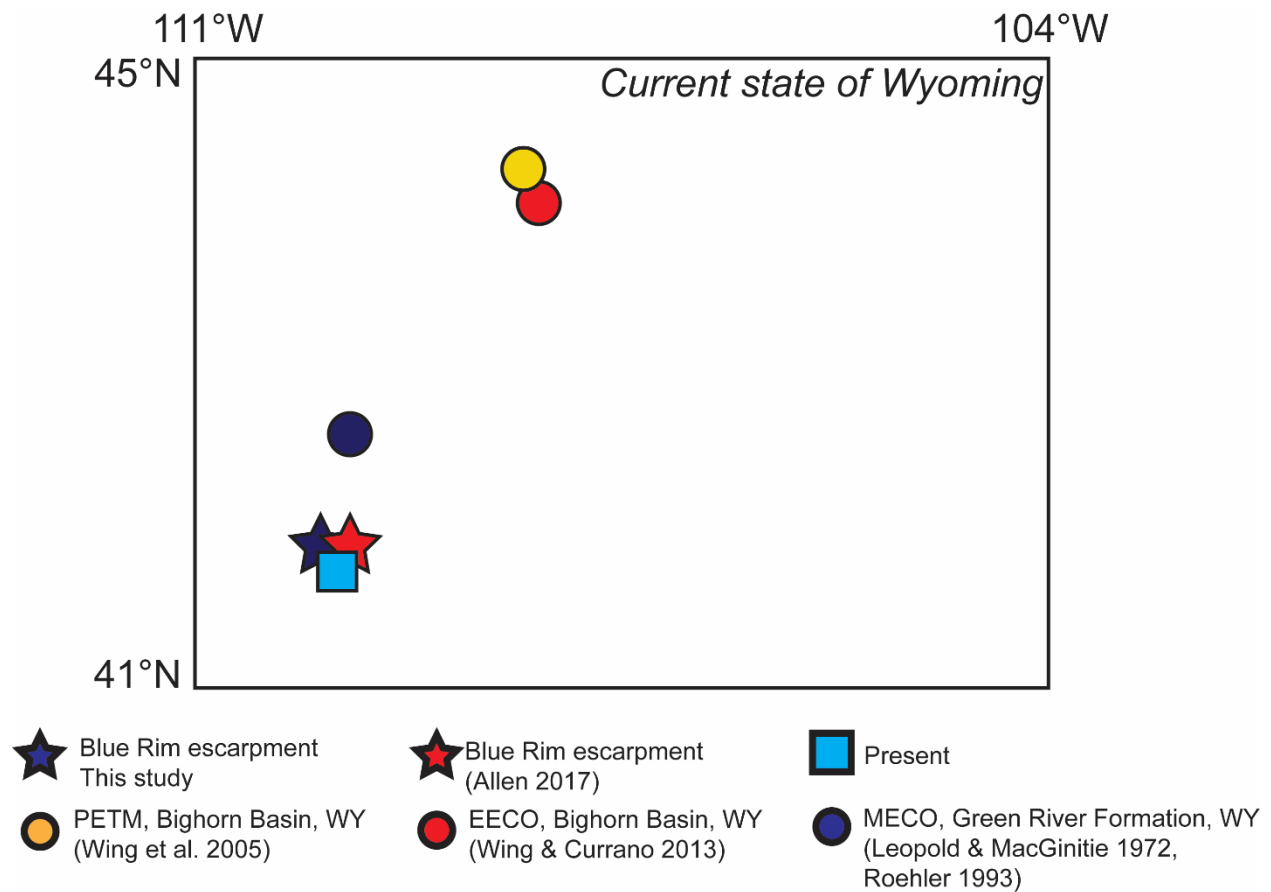


Figure S7 Current boundaries of Wyoming, USA with localities plotted with same symbols as seen in Figure 10. Blue Rim escarpment is plotted in stars (blue for this study, red for Allen 2017b). The Paleocene–Eocene Thermal Maximum record from Bighorn Basin is plotted in a yellow circle, while the EECO record from the Bighorn Basin is plotted in a red circle. The middle Eocene climatic optimum (MECO) is plotted in a blue circle.

Supplemental Methods:

Floral humidity province

To contextualize climate variables (temperature, precipitation) to ecoregion and humidity, Gulbranson et al. (2011) developed a life-zone proxy based on Rasmussen et al. (2005) and Rasmussen and Tabor's (2007) pedogenic energy model. This energy quantifies energy influxes due to solar radiation (and subsequent net primary productivity: NPP) and precipitation. The total energy input into a soil (E_{in}) is related to energy supplied by NPP (E_{NPP}) and precipitation (E_{PPT}). E_{PPT} and E_{NPP} are calculated using weathering indices (CIA). E_{PPT} is plotted against evapotranspiration (ET) and divided into humidity zones using Eq. 9:

$$\text{Equation (9)} \quad ET = MAP - E_{PPT} [4.18(\Delta T)]^{-1}$$

Where ΔT is the temperature difference between 273.16 °K and mean annual temperature.

Mean annual precipitation calculated using the relationship between CIA-K and precipitation was used in this relationship (Eq. 5).

In modern environments, effective precipitation (P_{eff}) is a linear function of MAP and ET (Eq. 10):

$$\text{Equation (10)} \quad P_{eff} = MAP - ET$$

And P_{eff} can be calculated using Eq. 11.

$$\text{Equation (11)} \quad P_{eff} = 0.9075(MAP) - 21.403$$

Paleolatitude has been described as anywhere between 35 °N and 44 °N (Allen 2017b), which is necessary criteria for determining the best equation for E_{NPP} in Gulbranson et al.'s (2011) model, though temperature can be swapped out as the best fit criteria. Temperature has been described as 17-20 °C by prior studies for this region during this time (Allen 2017b), so we use Eq. 12 determined by ranges of MAT in Gulbranson et al. (2011).

$$\text{Equation (12)} \quad E_{NPP} = -1.943(CIA)^2 + 352.41(CIA) + 28197$$

For reconstructed MAT and MAP values from alternate proxy data (non-paleosol estimates), CIA was back calculated estimating CIA-K using given precipitation values and Eq. 5, then translated into CIA values using Eq. 13.

This relationship was calculated using the relationship between CIA and CIA-K for all paleosol bulk geochemistry measurements at this site (Supplemental Fig. S1; $R^2 = 0.99$)

$$\text{Equation (13)} \quad CIA = 0.78(CIA - K) + 5.23$$

Holdridge Life Zones

The Holdridge Life Zone classification system (Holdridge 1947) matches climate with vegetation. Higher precipitation adds energy to a soil system, which mobilizes elements and weathers the soil. Evapotranspiration, represented on the other axis of the Holdridge biome diagram (Fig. 7b) represents energy loss from the soil profile. These two plotted together can then be divided into biome space, allowing for estimation of climate and vegetation through the same diagram. Using the ratio of evapotranspiration (calculated by Equation 10) to mean annual

precipitation, which represents potential evapotranspiration ratio, as compared to precipitation, we plotted each paleosol in life zones.

Global context of climate

Chronologically, the region of interest (specifically, the Rocky Mountain Wyoming region) went from wettest during the PETM in the proximal Bighorn Basin (rain forest; reconstructed using LMA and LAA; Wing et al. 2005) to drier and cooler (characterized as a wet forest), resulting in less evapotranspiration and less precipitation as time progressed. Blue Rim-era floral humidity provinces are all estimated to also be wet forests, which is further contextualized by fossil evidence as presented in the taxonomy and floral humidity provinces of our fossils and Allen's (2017) characterization of the escarpment. Other comparably aged Eocene climate reconstructions based on palynological data from the Laney Member of the Green River Formation (~48.5 Ma; Smith et al., 2008), located in the same basin as the Blue Rim escarpment, appear to be closer to rainforest floral humidity provinces (Leopold & MacGinitie 1972; Roehler 1993; Smith et al., 2008; Fig. 8). That being said, megafloora from the Green River Formation has been described as ranging from littoral to floodplain vegetation along the lakes edges, plants adapted to subhumid conditions slightly higher, broad-leaf deciduous trees in cooler and mesic situations, and conifer-hardwood and montane zones from high altitude regions (MacGinitie 1969). Over the late Paleogene into Neogene and more recently, the region has continued drying and is now high desert/dry scrub, with minimal precipitation (195 mm yr⁻¹ in 2019, the year sampled; PRISM Climate Group 2004), cold winters (<0 °C from November to March; PRISM Climate Group 2004), and hot, dry summers (Fig. 8). The locations of each of these sites is plotted on Figure S7, to demonstrate their proximity.

The Parachute Creek, Laney, and Fossil Butte Members of the Green River Formation, all slightly older than the Blue Rim escarpment and deposited during the EECO, have also been interpreted as semi-deciduous with seasonally dry subtropical taxa (Wing 1987; Allen 2015). Further away in the Okanagan Highlands of the North American Pacific Northwest, climate reconstructions yield temperature ranges of 10–13.5 °C (Wolfe et al. 1994; Wolfe et al. 1998; Greenwood et al. 2005), similar to those values reconstructed at Blue Rim, demonstrating the equability of North America during the early Eocene.

Blue Rim climate based on floral vs paleosol reconstructions

Mean annual precipitation (MAP) reconstructions from this study based on inorganic proxies in paleosols ranged from 608–1167 mm yr⁻¹ (average: 845 mm yr⁻¹ ± 255 mm yr⁻¹, standard deviation). A high influence of carbonate in the parent material resulted in a lower CIA-K, and thus lower rainfall estimates (Sheldon et al. 2002). Error on CIA-K proxies is ± 181 mm yr⁻¹ (Sheldon et al. 2002; Passchier et al. 2013), such that estimates from organic, physiognomic, and inorganic geochemical proxies are within error of one another. However, overall, these inorganic-based reconstructions are slightly lower than those estimated using Climate Leaf Analysis Multivariate Program (only in the lower horizon, CLAMP, 1653 ± 317 to 2070 ± 483 mm yr⁻¹; Allen 2017b) and leaf area analysis, which was estimated using four different regression equations based on different regions of today's world (LAA; ranging from 1299.4 + 563, -393 to 1539.8 + 1294, -703 depending on the regression used in the upper horizon: and 1454.8 + 358, -287 to 1711.0 + 1438, -781 depending on the regression used in UF-19404, isolated channel fill and oldest stratigraphically; Wilf et al. 1998; Gregory-Wodzicki 2000; Jacobs 2004; Peppe et al., 2011; Allen 2017b). This could be due to the location in the section

(stratigraphically older, see Figure 5) of the studied paleosols. Temperature results based off inorganic geochemistry in paleosols in this study were slightly lower than those reconstructed using leaf physiognomy (CLAMP: 14 to 15 °C, LMA: 14 to 20 °C; Fig. 7; Allen 2017b, originally calculated using Wolfe 1979; Wing and Greenwood 1993; Wilf 1997; Kowalski & Dilcher 2003; Miller et al., 2006; Spicer et al., 2009; and Peppe et al., 2011), with PWI-based temperatures ranging from 10 to 12 °C (average $11.0\text{ °C} \pm 0.7\text{ °C}$ standard deviation; Fig. 7).